Electronic Supplementary Material (ESI) for Physical Chemistry Chemical Physics.

Molecular mechanism relating with binding of fluorophores to Mango-II revealed by multiple-replica molecular dynamics simulations

Junxiao Chen[1,2], Na Li[1], Xingyu Wang[3], Jianzhong Chen[4*], John Z. H. Zhang[1,3] and Tong Zhu[1,3,5*]

[1]Shanghai Engineering Research Center of Molecular Therapeutics & New Drug Development, School of Chemistry and Molecular Engineering, East China Normal University, Shanghai, People's Republic of China.

[2]School of Chemistry and Pharmaceutical Engineering, Qilu University of Technology, Jinan, 250353, People's Republic of China

[3]NYU-ECNU Center for Computational Chemistry at NYU Shanghai, Shanghai, People's Republic of China

[4]School of Science, Shandong Jiaotong University, Jinan 250357, People's Republic of China

[5]Shandong Key Laboratory of Biophysics, Institute of Biophysics, Dezhou University, Dezhou 253023, China

[*] To whom correspondence should be addressed. Email: tongzhu.work@gmail.com; tzhu@lps.ecun.cn
Correspondence may also be addressed to Jianzhong Chen. Email: jzchen@sdjtu.edu.cn; chenjianzhong1970@163.com

File S1. Calculations of cross-correlation map

By now, the cross-correlation map has been an efficient approach to explore internal dynamics of receptors, rationally uncovering the details of motions of a nucleotide relative to the other nucleotides in the Mango-II RNA aptamer. The cross-correlation coefficient C_{ij} between C1'□ atoms *i* and *j* in nucleotides is computed using the structural ensembles saved in MRMD trajectories based on the following equation (1,2)

$$C_{ij} = \frac{< \Delta r_i \cdot \Delta r_j >}{(< \Delta r_i^2 >< \Delta r_j^2 >)^{1/2}}$$

(1)

where Δr_i represents the displacement of the *i*th C1' atom relative to its averaged position. The values of the cross-correlation coefficient C_{ij} change from -1 to 1. Usually, the positive values of C_{ij} represents the positively correlated motions of the nucleotides *i* relative to *j*, on the contrary the negative values of C_{ij} describe the anticorrelated movements between the nucleotides *i* and *j*. For the current study, the CPPTRAJ program(3) in AMBER was utilized to calculate the cross-correlation maps between nucleotides. To better identify the motion modes in the Mango-II RNA aptamer, the color-coded mode was adopted to visualize the extent of correlated motions between nucleotides.

File S2. Calculations of MM-GBSA

Molecular mechanics Poisson-Boltzmann surface area (MM-PBSA) and molecular mechanics generalized born surface area (MM-GBSA) are considered as two powerful methods to fast calculate binding free energies (4-6). Based on reliable comparison and evaluation of Hou's group (7,8) on the performance of these two methods, MM-GBSA method was utilized to compute binding free energies of two fluorophores TO1 and TO3 to the Mango-II RNA aptamer according to the following equation

$$\Delta G_{bind} = G_{comp} - G_{RNA} - G_{fluo} = \Delta E_{ele} + \Delta E_{vdW} + \Delta G_{pol} + \Delta G_{nonpol} - T\Delta S \quad (2)$$

in which G_{comp}, G_{RNA} and G_{fluo} indicate free energies of the complex, the Mango-II RNA aptamer and fluorophore, separately. The two terms ΔE_{ele} and ΔE_{vdW} represent electrostatic and van der Walls interactions of fluorophores with the Mango-II RNA aptamer, respectively. ΔG_{pol} and ΔG_{nonpol} independently correspond to the polar and nonpolar solvation free energies, among which ΔG_{pol} can be estimated by using the GB model developed by Onufriev et al. (9) and ΔG_{nonpol} is calculated with the empirical equation:

$$\Delta G_{nonpol} = \gamma \times \Delta SASA + \beta \quad (3)$$

where the parameters γ and $\Delta SASA$ separately represent the surface tension and the difference in the solvent accessible surface areas induced by ligand associations. The parameters γ and β were assigned as 0.0072 kcal·mol·Å^{-2} and 0 kcal·mol^{-1} in this work (10), separately. The last term $-T\Delta S$ indicates the contribution of the entropy change to binding free energies and is obtained by utilizing the mmpbsa_py_nabnmode program based on 50 structural frames (11).

Table S1 binding free energies of fluorophores to the Mango-II RNA calculated by MM-GBSA[a]

Components	TO1-WT RNA	TO1-A22U RNA	TO3-WT RNA	TO3-A22U RNA
ΔE_{ele}	-27.42±0.78[b]	-40.87±0.84	-24.80±0.75	-24.89±0.53
ΔE_{vdW}	-46.71±0.48	-49.09±0.25	-44.18±0.31	-44.44±0.25
ΔG_{pol}	55.91±0.74	68.50±0.76	46.95±0.41	47.02±0.55
ΔG_{nonpol}	-2.70±0.02	-2.73±0.01	-2.41±0.01	-2.52±0.02
[c]ΔH	-20.92±0.32	-24.19±0.22	-24.45±0.25	-24.83±0.23
[d]$T\Delta S$	12.97±0.41	14.04±0.21	17.18±0.33	18.32±0.45
ΔG_{bind}	-7.95	-10.15	-7.27	-6.51

[a]All values are in kcal/mol. [b]The symbols ± indicate standard errors of means.
[c]$\Delta H = \Delta E_{ele} + \Delta E_{vdW} + \Delta G_{pol} + \Delta G_{nonpol}$. [d]$\Delta G_{bind} = \Delta H - T\Delta S$.

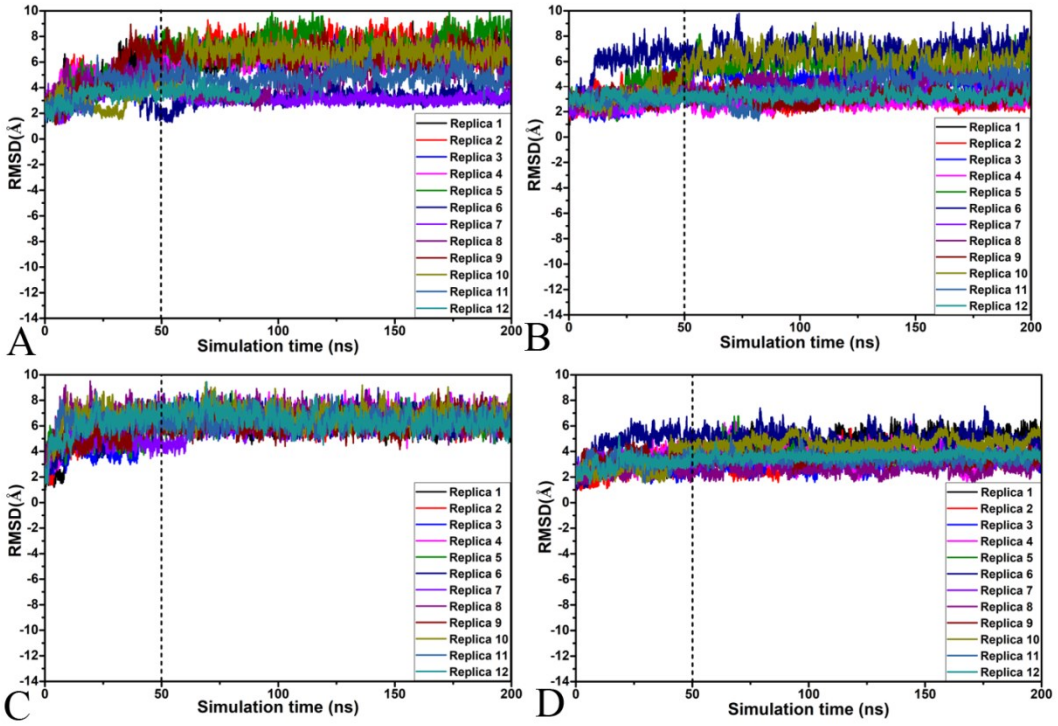

Fig. S1 Root mean square deviations (RMSDs) of atoms P, O3′, O5′ C3′, C4′ and C5′ in the Mango-II throughout the entire MRMD simulations consisting of 12 replicas: (A) the TO1-WT Mango-II, (B) the TO1-A22U mutated Mango-II, (C) the TO3-WT Mango-II and (D) the TO3-A22U mutated Mango-II.

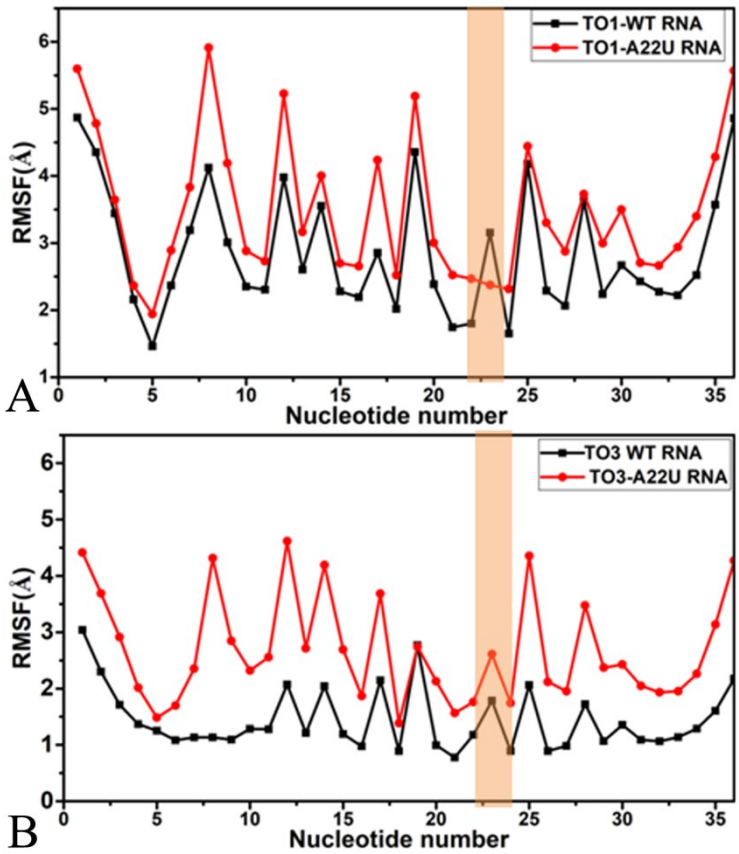

Fig. S2 Root-mean-square fluctuations (RMSFs) of the atoms C1' in nucleotides of the Mango-II VS the sequence number: (A) the WT and mutated Mango-II complexed with TO1 and (B) the WT and mutated Mango-II complexed with TO3.

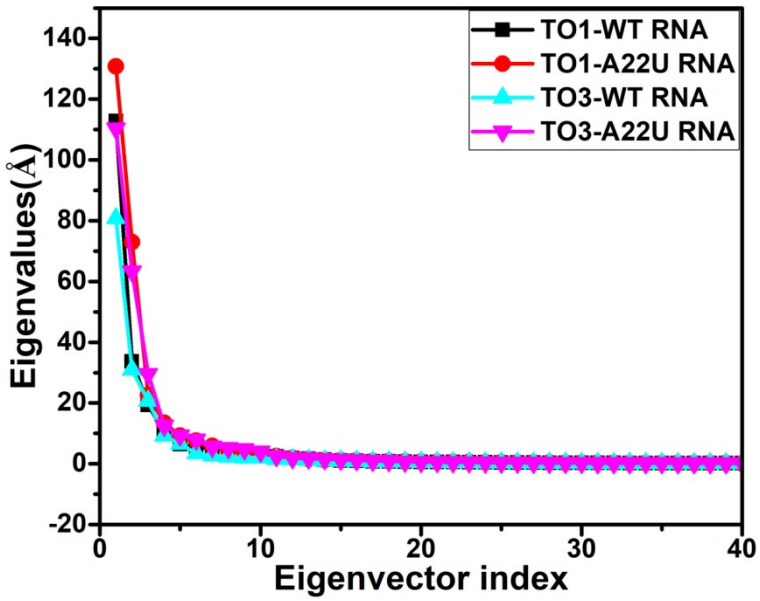

Fig. S3 The eigenvalues against the corresponding eigenvector indices generated by diagonalizing the covariance matrix of the C1' atoms in the Mango-II built by using the single joined MRMD trajectories.

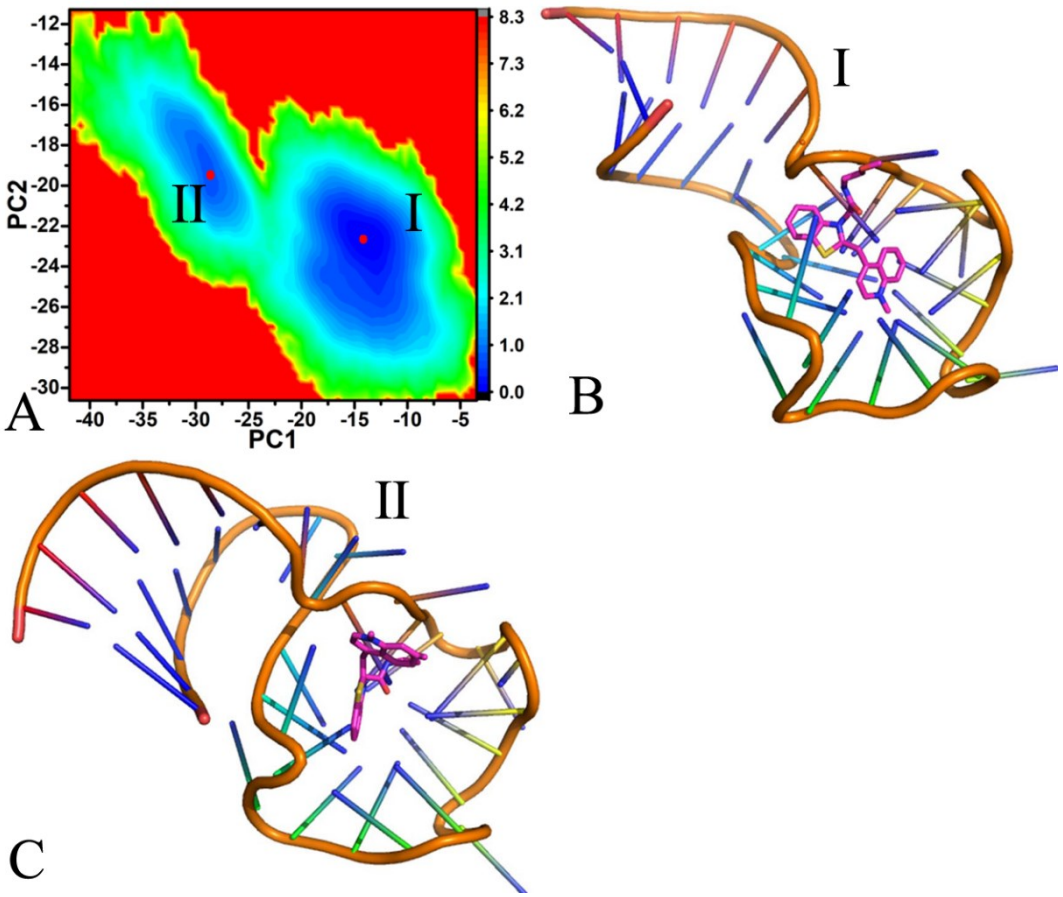

Fig. S4 Free energy landscape and molecular structures: (A) free energy landscape of the WT Mango-II with TO1 constructed by using projections of the single joined MRMD trajectory on the first two eigenvectors, (B) and (C) separately corresponding to the structures located in the energy basins Ⅰ and Ⅱ. The Mango-II is depicted in cartoon modes and TO1 indicated in stick modes.

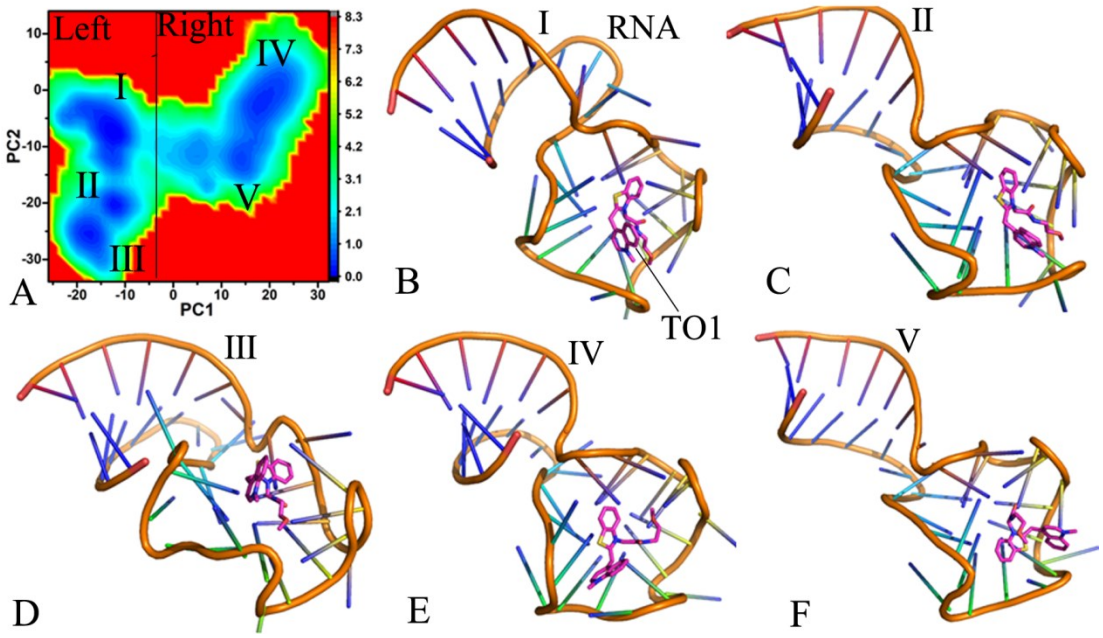

Fig. S5 Free energy landscape and molecular structures: (A) free energy landscape of the A22U mutated Mango-II with TO1 constructed by using projections of the single MRMD trajectory on the first two eigenvectors, (B), (C), (D), (E) and (F) respectively corresponding to the structures located in the energy basins Ⅰ, Ⅱ, Ⅲ, Ⅳ and Ⅴ. The Mango-II is shown in cartoon modes and TO1 displayed in stick modes.

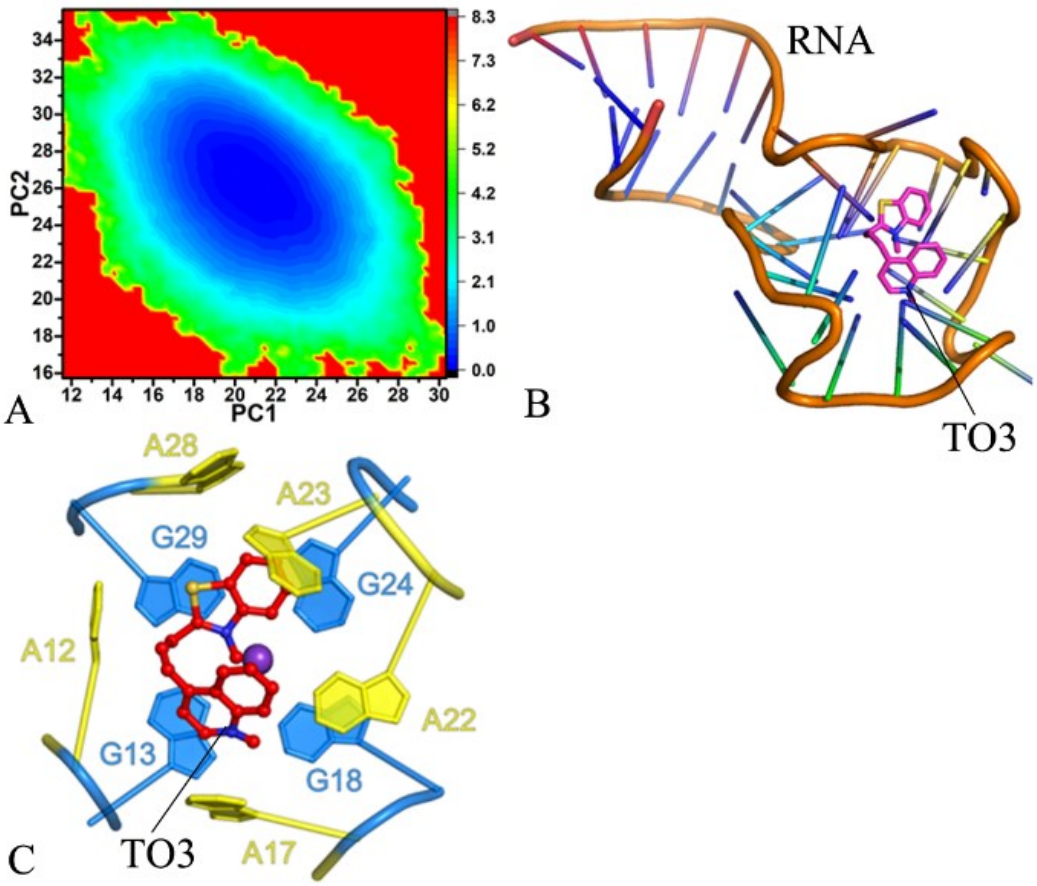

Fig. S6 Free energy landscape and molecular structures: (A) free energy landscape of the WT Mango-II with TO3 constructed by using projections of the single joined MRMD trajectory on the first two eigenvectors, (B) molecular structures of the WT Mango-II with TO3 located at energy basin, among which the Mango-II is characterized in cartoon modes and TO3 reflected in stick modes and (C) binding pocket around TO3, in which the RNA and TO3 are displayed in surface modes and stick modes, respectively.

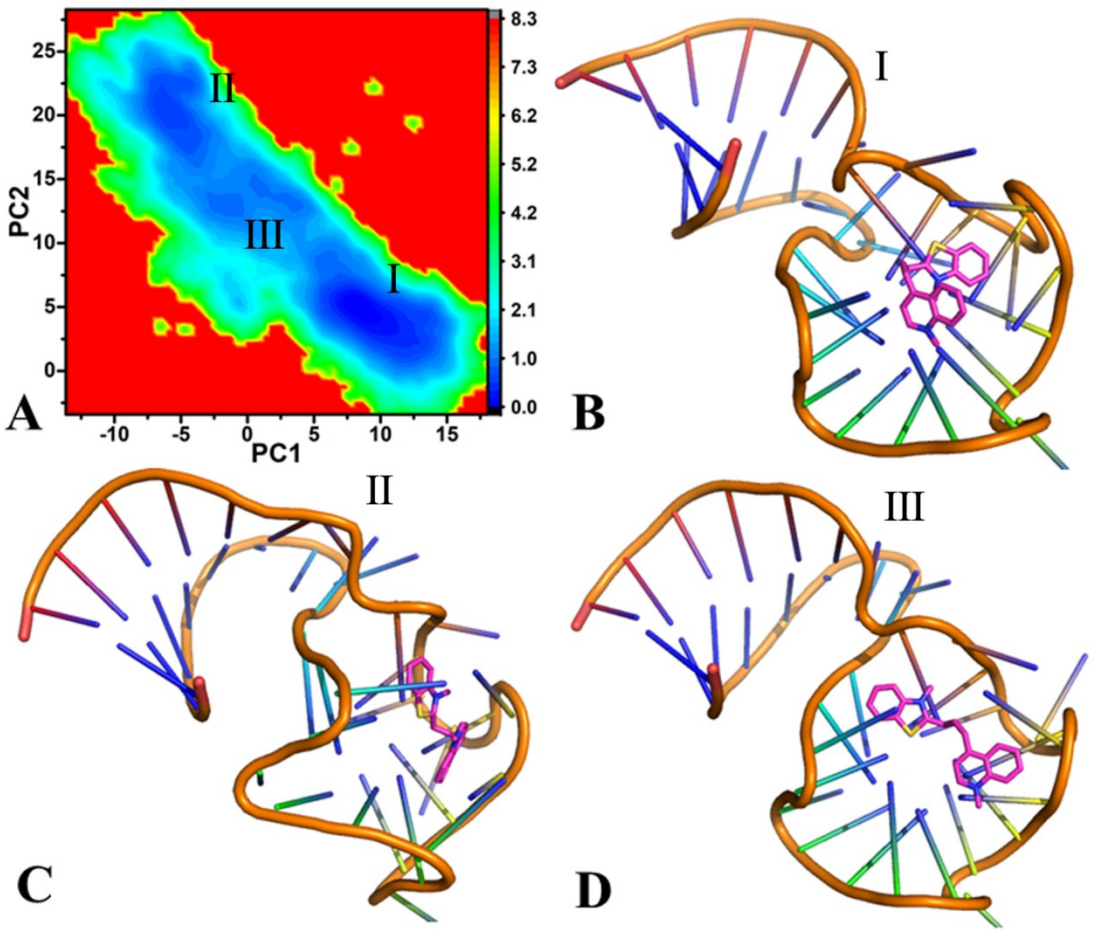

Fig. S7 Free energy landscape and molecular structures: (A) free energy landscape of the A22U mutated Mango-II with TO3 built by using projections of the single joined MRMD trajectory on the first two eigenvectors, (B), (C) and (D) respectively corresponding to the structures sited in the energy basins Ⅰ, Ⅱ and Ⅲ. The Mango-II and TO3 are depicted in cartoon modes and stick modes, separately.

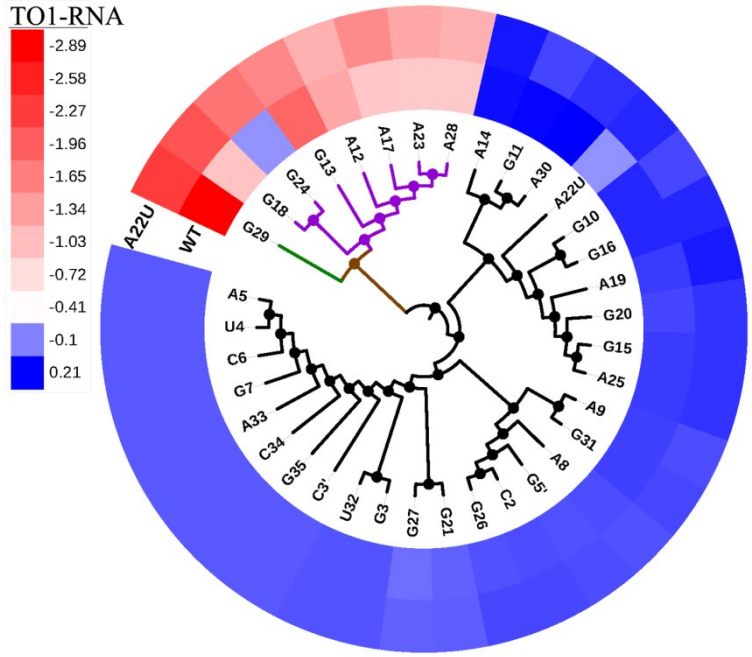

Fig. S8 Hierarchical clustering tree of nucleotides playing different roles in bindings of the fluorophore TO1 to the WT and mutated Mango-II based on energetic contributions of separate nucleotides. Energy contributions favoring the TO1 association are shown in red, with the highest contribution (-2.89 kcal/mol) is indicated by the exact red and lower contributions gradually fading towards the white (an indicator of -0.41 kcal/mol). Nevertheless, energy contributions weakening the TO1 associations are reflected by the blue, with the highest contributions (0.21 kcal/mol) are presented by the exact blue and lower ones gradually fading towards the white.

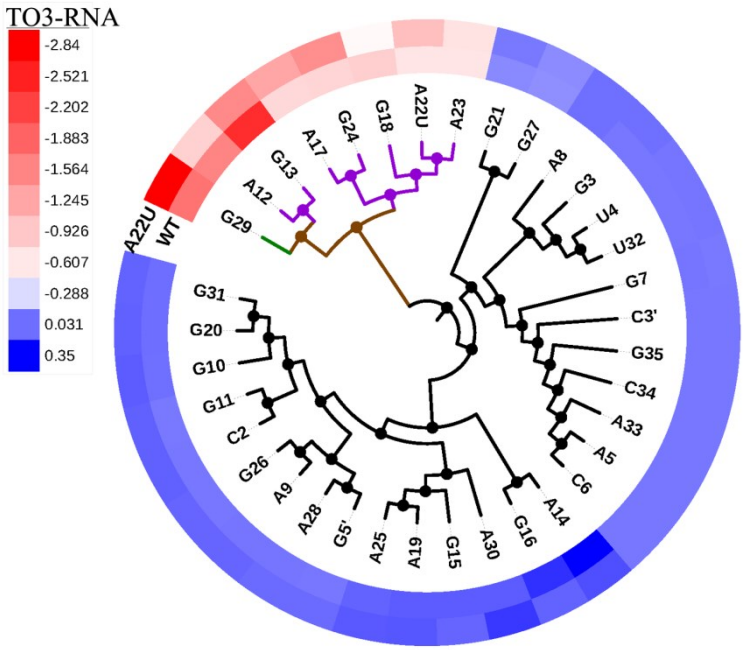

Fig. S9 Hierarchical clustering tree of nucleotides responsible for different contributions to identification of hot interaction spots of the fluorophore TO3 with the WT and mutated Mango-II based on energetic contributions of separate nucleotides. Energy contributions favoring the TO3 association are shown in the red, with the highest contribution (-2.84 kcal/mol) is reflected by the exact red and lower contributions gradually fading towards the white (an indicator of -0.41 kcal/mol). While the energetic contributions weakening the TO3 association are indicated by the blue, with the highest contributions (0.35 kcal/mol) are presented by the exact blue, and the lower ones gradually fading towards the white.

References

1. Ichiye, T. and Karplus, M. (1991) Collective motions in proteins: A covariance analysis of atomic fluctuations in molecular dynamics and normal mode simulations. *Proteins*, **11**, 205-217.
2. Chen, J., Pang, L., Wang, W., Wang, L., Zhang, J.Z.H. and Zhu, T. (2019) Decoding molecular mechanism of inhibitor bindings to CDK2 using molecular dynamics simulations and binding free energy calculations. *J. Biomol. Struct. Dyn.*, 1-12.
3. Roe, D.R. and Cheatham, T.E. (2013) PTRAJ and CPPTRAJ: Software for Processing and Analysis of Molecular Dynamics Trajectory Data. *J. Chem. Theory Comput.*, **9**, 3084-3095.
4. Wang, W. and Kollman, P.A. (2000) Free energy calculations on dimer stability of the HIV protease using molecular dynamics and a continuum solvent model. *J. Mol. Biol.*, **303**, 567-582.
5. Wang, W. and Kollman, P.A. (2001) Computational study of protein specificity: The molecular basis of HIV-1 protease drug resistance. *Proc. Natl. Acad. Sci. U. S. A.*, **98**, 14937-14942.
6. Wang, J., Morin, P., Wang, W. and Kollman, P.A. (2001) Use of MM-PBSA in Reproducing the Binding Free Energies to HIV-1 RT of TIBO Derivatives and Predicting the Binding Mode to HIV-1 RT of Efavirenz by Docking and MM-PBSA. *J. Am. Chem. Soc.*, **123**, 5221-5230.
7. Sun, H., Li, Y., Shen, M., Tian, S., Xu, L., Pan, P., Guan, Y. and Hou, T. (2014) Assessing the performance of MM/PBSA and MM/GBSA methods. 5. Improved docking performance using high solute dielectric constant MM/GBSA and MM/PBSA rescoring. *Phys. Chem. Chem. Phys.*, **16**, 22035-22045.
8. Sun, H., Li, Y., Tian, S., Xu, L. and Hou, T. (2014) Assessing the performance of MM/PBSA and MM/GBSA methods. 4. Accuracies of MM/PBSA and MM/GBSA methodologies evaluated by various simulation protocols using PDBbind data set. *Phys. Chem. Chem. Phys.*, **16**, 16719-16729.
9. Onufriev, A., Bashford, D. and Case, D.A. (2004) Exploring protein native states and large-scale conformational changes with a modified generalized born model. *Proteins*, **55**, 383-394.
10. Gohlke, H., Kiel, C. and Case, D.A. (2003) Insights into Protein–Protein Binding by Binding Free Energy Calculation and Free Energy Decomposition for the Ras–Raf and Ras–RalGDS Complexes. *J. Mol. Biol.*, **330**, 891-913.
11. Miller, B.R., McGee, T.D., Swails, J.M., Homeyer, N., Gohlke, H. and Roitberg, A.E. (2012) MMPBSA.py: An Efficient Program for End-State Free Energy Calculations. *J. Chem. Theory Comput.*, **8**, 3314-3321.